The Arlequin method as a flexible engineering design tool

Hachmi Ben Dhia, Guillaume Rateau

▶ **To cite this version:**

Hachmi Ben Dhia, Guillaume Rateau. The Arlequin method as a flexible engineering design tool. International Journal for Numerical Methods in Engineering, 2005, 62 (11), pp.1442-1462. 10.1002/nme.1229 . hal-04704957

HAL Id: hal-04704957
https://hal.science/hal-04704957v1

Submitted on 11 Oct 2024

HAL is a multi-disciplinary open access archive for the deposit and dissemination of scientific research documents, whether they are published or not. The documents may come from teaching and research institutions in France or abroad, or from public or private research centers.

L'archive ouverte pluridisciplinaire **HAL**, est destinée au dépôt et à la diffusion de documents scientifiques de niveau recherche, publiés ou non, émanant des établissements d'enseignement et de recherche français ou étrangers, des laboratoires publics ou privés.

Distributed under a Creative Commons Attribution - NonCommercial 4.0 International License

The Arlequin method as a flexible engineering design tool

Hashmi Ben Dhia[*,†] **and Guillaume Rateau**

Laboratoire MSS-Mat, Unité Mixte de Recherche, 8579 CNRS, École Centrale Paris, Châtenay-Malabry, France

By superposing and gluing models, the Arlequin method offers an extended modelling framework for the design of engineering structures. This paper aims at developing the numerical aspects of the approach and at showing how it can be used with great flexibility and in a consistent manner to change locally a global mechanical model. The capabilities of the Arlequin method and the effectiveness of the implemented numerical tools are exemplified by 1-D, 2-D and 3-D numerical applications.

KEY WORDS: multimodel; multiscale; partition of unity; substructuring; overlapping; Arlequin method

1. INTRODUCTION

Changing locally a globally defined mechanical or numerical model while saving human and machine resources is essential in the designing and analysing of engineering structures. Indeed, it is of primary importance to be able

- to introduce with great flexibility local defects (such as cracks, holes or inclusions) in a global existing *coarse* model,
- to change the local behaviour in a globally simplified modelling of a given material (e.g. to substitute a large deformation elastoplastic behaviour for a linearized elastic one),
- to relax hypotheses like classical continuum mechanics ones in the neighbourhood of some critical points in order to better fit physical phenomena of interest, ...

From the computational standpoint, one of the main difficulties to achieve this task lies in the lack of flexibility of classical numerical tools such as the finite element method (FEM) and more precisely to cumbersome technical aspects related to local refinement.

*Correspondence to: H. B. Dhia, Laboratoire MSS-Mat, Unité Mixte de Recherche, 8579 CNRS, École Centrale Paris, Châtenay-Malabry, France.
†E-mail: bendhia@mssmat.ecp.fr

Contract/grant sponsor: Électricité de France

Accepted Manuscript

Important innovative and efficient numerical methods have been developed during the last decade to improve the flexibility of the FEM. Let us mention in particular the diffuse and meshless methods [1, 2], the mixing FEM/MLS [3], the volume correction multiscale approaches [4–7], the partition of unity method [8, 9], the GFEM [10], the X-FEM [11–13], and very recently the IEM [14] which is closely related to the mixing FEM/MLS. These approaches are basically *monomodel* and may either lack flexibility or relevance to address the above issues. The s-method of Fish [15] (see also References [16–19]) stands for another numerical tool of local–global type that is relevant in practice. It superimposes additional local and refined meshes to an existing global one, thus allowing different modelling in the superimposed meshes.

Like the s-method, the Arlequin method [20, 21] aims at creating a multimodel framework. However the models are not *added* but *crossed* and *glued* to each others. More precisely, it consists in

1. a superposition of mechanical states in a subzone, denoted as S (and here assumed to be known), of the whole domain Ω occupied by the mechanical system;
2. an energy distribution between the mechanical states in S, by using weight functions (building a partition of unity) in order to conserve the local mechanical energies;
3. a weak and compatible gluing of these states in S, or more generally in a subzone of S we call the gluing zone.

When compared to the s-method, the Arlequin method requires higher costs due to both (i) the treatment of the gluing of the superimposed mechanical states and the possible introduction of a Lagrange multiplier field associated to an interface coupling operator as in hybrid formulations [22] or dual domain decomposition methods (e.g. References [23, 24]), and (ii) the distribution of energies in the superposition zone which locally affects the stiffness matrices even in the linear framework. However it has no redundancy problem and is definitely *multimodel* since not only displacement fields but also complete mechanical states are potentially allowed to concurrently exist in the superposition zone.

Since based on superposition of models, the Arlequin method may recall the overset grid methods (also known as Chimera methods) introduced by the computational fluid community (e.g. Reference [25]) to improve the efficiency of the finite difference method in solving fluid problems in complex geometries. As a matter of fact, these methods are closely related to the overlapping Schwarz methods [26] stemming from the classical alternating Schwarz algorithm. The latter, originally designed to establish existence results for partial differential equations, has been extended in the form of a relevant substructuring method to solve large-sized discrete mechanical problems in parallel machines. However, the overlapping Schwarz method may not seem to be in essence the most appropriate tool to address the above multimodel or multiscale issues.

Domain superposition and energy averaging have been also used within the applied mathematics community to derive models for joined multi-structures through asymptotic approaches ([27, 28] and the reference therein) and within the computational physics community by Abraham *et al.* [29] to couple atomistic, molecular and continuum mechanics scales. Incidently, the methodology developed in Reference [29] is quite similar to the Arlequin methodology [20] though the couplings of models or scales are significantly different. The two methodologies seem to have been developed concurrently.

In the Arlequin framework, the mechanical states in the superposition subzone are defined as the *partition* of the superimposed states. The partitioned fields are labelled as *Arlequin*

Accepted manuscript

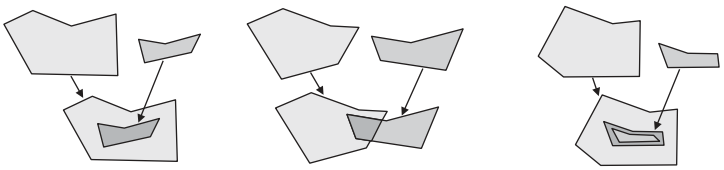

Figure 1. Modelling actions.

fields. In addition, the fact that models are locally crossed with each others theoretically allows the coexistence of substantially different mechanical and numerical models. Iteration of the crossing process [21] (by taking care of multiple gluings) can potentially lead to some relevant multiscale models.

The Arlequin method hence offers a framework to mix and glue different models with others. Three different modelling actions can be combined (see Figure 1 where the darkest areas stand for the gluing zones):

- Locally refine models (*zoom*)
- Link structure models (*substructuring or external junction*)
- Introduce an essential local modification in models (*internal junction*)

The possible discrepancy between the scales of the local and global models in the gluing zone need to be addressed with sufficient care. Many coupling operators have been suggested in previous papers by Ben Dhia [20, 21]. Some of these operators have been theoretically proved in References [30, 31] to be particularly well-suited, in the sense that they lead to well-posed continuous and discrete problems (at least in the linear elasticity framework), the latter being also well-conditioned.

A second aspect of the approach is related to the fact that by construction, the Arlequin framework allows the coexistence of incompatible models, sharing the energies of the system in the superposition regions and linked to each other in an appropriate way in the gluing subregions. These unusual energy distributions, both with a more common introduction of coupling of incompatible models (e.g. References [15, 18, 32, 33]), require special numerical and technical developments.

In the present paper, we focus on these last aspects. We first recall the continuous and the discrete mixed Arlequin equations for a model elasticity problem and some theoretical results stating the well-posedness of these formulations. In Section 3, the discretization by means of the finite element method and the related implementation concerns are investigated. The capabilities of the Arlequin method and the effectiveness of the choices of some of its components and their numerical integration are exemplified by selected 1-D, 2-D and 3-D numerical applications given in the last section.

2. A MIXED ARLEQUIN FORMULATION

The Arlequin formulations and some related theoretical results are recalled for completeness.

Accepted Manuscript

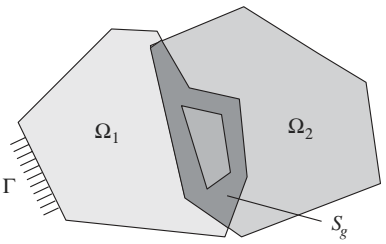

Figure 2. Superimposed domains and the gluing zone S_g.

2.1. Continuous formulations

In order to introduce Arlequin equations, we consider a static linearized elasticity problem defined in a polyhedral domain Ω. We let Γ, $\mathbf{f}$, $\boldsymbol{\varepsilon}(\mathbf{v})$ and $\boldsymbol{\sigma}(\mathbf{v})$, respectively, denote the clamped part of the boundary $\partial\Omega$, the applied density of body forces, the linearized strain and stress tensors associated to the displacement field $\mathbf{v}$. Without restriction, the complementary part of Γ in $\partial\Omega$ is assumed to be free. We also assume that the constitutive material follows a Hooke's law, which reads using usual convention of summation over repeated indices:

$$\boldsymbol{\sigma}_{ij}(\mathbf{v}) = \mathbf{R}_{ijkl}\boldsymbol{\varepsilon}_{kl}(\mathbf{v}) \tag{1}$$

The elasticity moduli $\mathbf{R}_{ijkl}$ are supposed to satisfy the classical symmetry, coercitivity and regularity hypotheses (see e.g. Reference [34]).

The classical displacement problem of the considered mechanical system then reads

$$\min_{\mathbf{v}\in\mathbf{W}} E(\mathbf{v}) \tag{2}$$

where, using classical notations,

$$\mathbf{W} = \{\mathbf{v} \in \mathbf{H}^1(\Omega);\ \mathbf{v} = \mathbf{0} \text{ on } \Gamma\} \tag{3}$$

$$E(\mathbf{v}) = \frac{1}{2}\int_\Omega \boldsymbol{\sigma}(\mathbf{v}) : \boldsymbol{\varepsilon}(\mathbf{v})\,\mathrm{d}\Omega - \int_\Omega \mathbf{f}.\mathbf{v}\,\mathrm{d}\Omega \tag{4}$$

To rewrite (2) according to the Arlequin *vision*, we consider that Ω is partioned into two overlapping polyhedral domains Ω_1 and Ω_2. The clamped part Γ is assumed to be, say, in $\partial\Omega_1$. We let S_g denote the gluing zone supposed to be a non-zero measured polyhedral subset of $S = \Omega_1 \cap \Omega_2$. It is assumed that the boundary of the superposition zone is contained in the boundary of the gluing zone (see Figure 2). To model the gluing forces, we use the choices analysed in Reference [30], for which we have good mathematical and numerical properties. As a matter of fact, the *natural* way to treat the *volume* gluing of displacement fields consists in activating Lagrange multiplier field belonging to the dual of the space of the admissible displacement fields restricted to S_g. This leads to a coupling operator based on a duality bracket between $\mathbf{H}^1(S_g)$ and its dual space [21]. At the discrete level, this duality bracket can be approximated by an $\mathbf{L}^2(S_g)$ scalar product. Another strategy is adopted hereafter and the two strategies will be compared for a 1-D test (see example 4.1).

Accepted Manuscript

By using the Riesz representation theorem, a natural scalar product of $\mathbf{H}^1(S_g)$ can be substituted (in an isomorphic way) to the duality bracket (e.g. Reference [35]). This choice generates both a well-posed mathematical problem and an easy-to-implement numerical operator. By the way, we notice that this last numerical aspect stands for an advantage of the *volume* coupling operator (intimately related to the structure of the Arlequin method) when compared to more usual surface couplings used for instance in mortar finite element methods [36–38].

Baring these elements in mind, the mixed Arlequin problem can be written as follows:

$$\min_{(\mathbf{v}_1,\mathbf{v}_2)\in\mathbf{W}_1\times\mathbf{W}_2}\ \max_{\boldsymbol{\lambda}\in\mathbf{W}_g}\ \{E_1(\mathbf{v}_1)+E_2(\mathbf{v}_2)+C(\boldsymbol{\lambda},\mathbf{v}_1-\mathbf{v}_2)\} \tag{5}$$

where

$$\mathbf{W}_1=\{\mathbf{v}_1\in\mathbf{H}^1(\Omega_1);\ \mathbf{v}_1=\mathbf{0}\ \text{on}\ \Gamma\} \tag{6}$$

$$\mathbf{W}_2=\mathbf{H}^1(\Omega_2) \tag{7}$$

$$\mathbf{W}_g=\mathbf{H}^1(S_g) \tag{8}$$

$$E_i(\mathbf{v}_i)=\frac{1}{2}\int_{\Omega_i}\alpha_i\,\boldsymbol{\sigma}(\mathbf{v}_i):\boldsymbol{\varepsilon}(\mathbf{v}_i)\,\mathrm{d}\Omega-\int_{\Omega_i}\beta_i\mathbf{f}.\mathbf{v}_i\,\mathrm{d}\Omega \tag{9}$$

$$C(\boldsymbol{\lambda},\mathbf{v})=\int_{S_g}\boldsymbol{\lambda}.\mathbf{v}+\ell^2\boldsymbol{\varepsilon}(\boldsymbol{\lambda}):\boldsymbol{\varepsilon}(\mathbf{v})\,\mathrm{d}\Omega \tag{10}$$

and where α_i, β_i and ℓ, respectively, denote two weight parameter functions and a strictly positive parameter homogeneous to a length. The weight parameter functions α_i and β_i are required not to count the energy in the overlap twice. They are assumed to be positive piecewise continuous functions in Ω_i and they satisfy the following equalities:

$$\alpha_1+\alpha_2=\beta_1+\beta_2=1\quad\text{in}\ S \tag{11}$$

$$\alpha_i=\beta_i=1\quad\text{in}\ \Omega_i\setminus S \tag{12}$$

Remark 1
In the superposition zone, distinct mechanical states concurrently exit. The stress tensor field actually satisfying the mechanical equilibrium is defined as the weighting of the stress tensor fields associated to both models through the α functions pair:

$$\boldsymbol{\sigma}^{\text{arl}}=\begin{cases}\boldsymbol{\sigma}(\mathbf{u}_1) & \text{in}\ \Omega_1\setminus S\\ \boldsymbol{\sigma}(\mathbf{u}_2) & \text{in}\ \Omega_2\setminus S\\ \alpha_1\boldsymbol{\sigma}(\mathbf{u}_1)+\alpha_2\boldsymbol{\sigma}(\mathbf{u}_2) & \text{in}\ S\end{cases} \tag{13}$$

As mentioned in the introduction, this field is labelled as Arlequin stress tensor field.

Accepted Manuscript

Remark 2
The coupling operator $C(.,.)$, defined by (10), is equivalent to the $\mathbf{H}^1(S_g)$ natural scalar product. The above mentioned $\mathbf{L}^2(S_g)$ scalar product is obtained by setting $\ell = 0$ in (10). In the sequel, it will be denoted by C_{L^2}.

2.2. Discrete formulations

The discrete formulations are derived from the continuous one by means of the finite element method. To this end, the domains Ω_1 and Ω_2 are, respectively, meshed by two sets of triangulations, denoted $(\mathscr{T}_{h_1})$ and $(\mathscr{T}_{h_2})$. The gluing zone is described by a set of triangulations, $(\mathscr{T}_{h_g})$, and we let $\mathbf{W}_{h_i} \subset \mathbf{W}_i$ denote the related conforming finite element spaces, for i varying in $\{1, 2, g\}$ (e.g. Reference [39]). That way, the discrete problems read:

$$\min_{(\mathbf{v}_{h_1},\mathbf{v}_{h_2})\in\mathbf{W}_{h_1}\times\mathbf{W}_{h_2}} \max_{\boldsymbol{\lambda}_{h_g}\in\mathbf{W}_{h_g}} \{E_1(\mathbf{v}_{h_1}) + E_2(\mathbf{v}_{h_2}) + C(\boldsymbol{\lambda}_{h_g}, \mathbf{v}_{h_1} - \mathbf{v}_{h_2})\} \tag{14}$$

The related Euler equations read

$$\text{Find } (\mathbf{u}_{h_1}, \mathbf{u}_{h_2}, \boldsymbol{\lambda}_{h_g}) \in \mathbf{W}_{h_1} \times \mathbf{W}_{h_2} \times \mathbf{W}_{h_g}$$

$$\forall \mathbf{v}_{h_1} \in \mathbf{W}_{h_1}, \quad \int_{\Omega_1} \alpha_1\, \boldsymbol{\sigma}(\mathbf{u}_{h_1}) : \boldsymbol{\varepsilon}(\mathbf{v}_{h_1})\, \mathrm{d}\Omega + C(\boldsymbol{\lambda}_{h_g}, \mathbf{v}_{h_1}) = \int_{\Omega_1} \beta_1 \mathbf{f}.\mathbf{v}_{h_1}\, \mathrm{d}\Omega \tag{15}$$

$$\forall \mathbf{v}_{h_2} \in \mathbf{W}_{h_2}, \quad \int_{\Omega_2} \alpha_2 \boldsymbol{\sigma}(\mathbf{u}_{h_2}) : \boldsymbol{\varepsilon}(\mathbf{v}_{h_2})\, \mathrm{d}\Omega - C(\boldsymbol{\lambda}_{h_g}, \mathbf{v}_{h_2}) = \int_{\Omega_2} \beta_2 \mathbf{f}.\mathbf{v}_{h_2}\, \mathrm{d}\Omega \tag{16}$$

$$\forall \boldsymbol{\mu}_{h_g} \in \mathbf{W}_{h_g}, \quad C(\boldsymbol{\mu}_{h_g}, \mathbf{u}_{h_1} - \mathbf{u}_{h_2}) = 0 \tag{17}$$

where we note that in (15) and (16), the second member of the left hand side terms stands for the virtual work of the gluing forces while (17) stands for the weak gluing system.

In Reference [30], we established that, under some classical hypotheses and some conditions which are rather easy to satisfy in practice (see Remark 3), the continuous and the discrete problems are well-posed. Moreover, the solutions of the continuous and discrete problems satisfy an optimal *a priori* error estimate. Basically, if $(\mathbf{u}_1,\ \mathbf{u}_2,\ \boldsymbol{\lambda})$ and $(\mathbf{u}_{h_1},\ \mathbf{u}_{h_2},\ \boldsymbol{\lambda}_{h_g})$ respectively denote the solutions of the continuous and discrete problems and if a sufficient regularity is assumed for the continuous fields then;

$$\exists C > 0 \text{ indepedent of } h_1, h_2 \text{ and } h_g$$

$$\|\mathbf{u}_1 - \mathbf{u}_{h_1}\|_{\mathbf{W}_1} + \|\mathbf{u}_2 - \mathbf{u}_{h_2}\|_{\mathbf{W}_2} + \|\boldsymbol{\lambda} - \boldsymbol{\lambda}_{h_g}\|_{\mathbf{W}_g} \leqslant C \max(h_1, h_2, h_g) \tag{18}$$

Remark 3
The additional conditions ensuring the theoretical results at the discrete level are the following:

$$\forall i \in \{1, 2\}, \exists \alpha_0 > 0;\ \alpha_i \geqslant \alpha_0 \text{ in } S \tag{19}$$

$$\mathbf{W}_{h_g} \subset \mathbf{W}_{h_1|S_g} \quad \text{or} \quad \mathbf{W}_{h_g} \subset \mathbf{W}_{h_2|S_g}$$
$$\text{where } \mathbf{W}_{h_i|S_g} \text{ stands for } \mathrm{span}\{\mathbf{v}_{|S_g};\ \forall \mathbf{v} \in \mathbf{W}_{h_i}\} \tag{20}$$

Accepted Manuscript

Condition (19) on the weight parameter functions α_i presents no practical difficulty. Moreover, the compatibility-like condition (20) may rather easily be satisfied in practice, as we demonstrate in the following section.

Remark 4
The weight functions, α_1 and α_2, are here assumed to be given. The Arlequin solution depends on these functions when two different numerical or mechanical models are superposed. Though an optimal choice of these functions seems to be a rather intricate issue, an operational one consists in relating their values to the relative local refinement of the associated models. This choice is partially confirmed by numerical investigations (see Section 4) and by theoretical limit results which will be published elsewhere. In addition, when considering deformable bodies, the stability analysis of problem (5) recalled above shows that each α_i must be strictly positive. However, in the particular case where a rigid body is superimposed to a deformable one, all the internal energy is supported by the deformable body. In these particular situations, one can notice the similarity between the fictitious domain method with a distributed Lagrange multiplier [40] and the (mixed) Arlequin method.

3. DISCRETIZATION AND IMPLEMENTATION ISSUE

In the previous sections, we stated that the Arlequin method offers an *a priori* relevant way to the (local) approximation of multiscale mechanical problems. However, to work out a robust and easy-to-use modelling tool, some computation issues have to be investigated.

3.1. Discretization framework

The Arlequin method can address a large number of combinations of superimposed models, kinematics, interpolations, meshes, ... For the sake of clarity, we hence restrict the following discussion to a minimal, but significant, framework.

As in the previous section, the overlapping of no more than two solid finite element models is considered. For a more convenient and efficient use of this method, we also assume that the related triangulations may be independent. Furthermore, the simplest parameterization of the weighting functions is chosen. Namely, those functions are taken equal to 1 outside the overlap and constant inside. The related constants are denoted by α_1^0, α_2^0, β_1^0 and β_2^0. Finally, we begin this discussion by assuming that $\mathscr{T}_{h_g}$ is independent of $\mathscr{T}_{h_1}$ and $\mathscr{T}_{h_2}$. Then, at the end of this section, we consider more practical possibilities related to condition (20).

3.2. Computation key point

Given this framework, we now focus on solving the discrete problems (15)–(17). To this end, we let $(\boldsymbol{\varphi}_1^i)$, $(\boldsymbol{\varphi}_2^j)$ and $(\boldsymbol{\varphi}_g^k)$ denote the finite element basis functions of $\mathbf{W}_{h_1}$, $\mathbf{W}_{h_2}$ and $\mathbf{W}_{h_g}$. The vectors $\mathscr{U}_1$, $\mathscr{U}_2$ and $\boldsymbol{\Lambda}$, respectively, stand for the co-ordinates of $\mathbf{u}_{h_1}$, $\mathbf{u}_{h_2}$ and $\boldsymbol{\lambda}_{h_g}$ in these bases. The discrete problem (15)–(17) is equivalent to the following linear

Accepted Manuscript

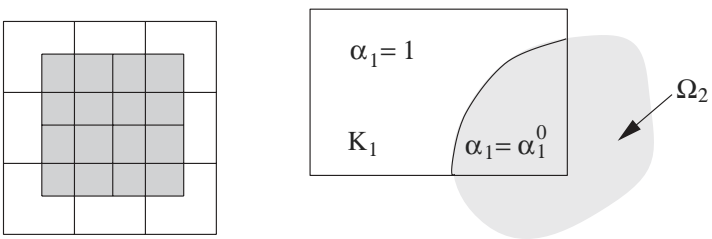

Figure 3. Heterogeneities at the element scale.

system:

$$\begin{bmatrix} \mathscr{K}_1 & \mathbf{0} & \mathscr{C}_1^{\mathrm{T}} \\ \mathbf{0} & \mathscr{K}_2 & -\mathscr{C}_2^{\mathrm{T}} \\ \mathscr{C}_1 & -\mathscr{C}_2 & \mathbf{0} \end{bmatrix} \begin{bmatrix} \mathscr{U}_1 \\ \mathscr{U}_2 \\ \mathbf{\Lambda} \end{bmatrix} = \begin{bmatrix} \mathscr{F}_1 \\ \mathscr{F}_2 \\ \mathbf{0} \end{bmatrix} \tag{21}$$

for which we need to evaluate

- the weighted stiffness matrices

$$(\mathscr{K}_i)_{jk} = \int_{\Omega_i} \alpha_i \boldsymbol{\sigma}(\boldsymbol{\varphi}_i^k) : \boldsymbol{\varepsilon}(\boldsymbol{\varphi}_i^j)\, \mathrm{d}\Omega \tag{22}$$

- the weighted loading vectors

$$(\mathscr{F}_i)_j = \int_{\Omega_i} \beta_i \mathbf{f}.\boldsymbol{\varphi}_i^j\, \mathrm{d}\Omega \tag{23}$$

- the coupling matrices

$$(\mathscr{C}_i)_{jk} = \int_{S_g} \boldsymbol{\varphi}_g^j.\boldsymbol{\varphi}_i^k + \ell^2 \boldsymbol{\varepsilon}(\boldsymbol{\varphi}_g^j) : \boldsymbol{\varepsilon}(\boldsymbol{\varphi}_i^k)\, \mathrm{d}\Omega \tag{24}$$

The mixed matrix in (21) is not positive definite. Many numerical strategies have been developed to efficiently solve such systems, particularly by the domain decomposition community (see e.g. Reference [23]). So we do not discuss this point any further.

As a matter of fact, the technical difficulty is related to geometrical incompatibilities. Indeed, since the meshes $\mathscr{T}_{h_1}$, $\mathscr{T}_{h_2}$ and $\mathscr{T}_{h_g}$ may be independent, they *a priori* do not match in the overlap (see Figure 3). Consequently, (22)–(24) should not be computed in the finite element classical way. The non-matching relation between the triangulations leads to *heterogeneous* integrands at the element scale, so that standard quadrature formulae, used in the reference finite elements, may generate spurious numerical oscillations of the solution fields. This implementation issue is also encountered by other methods (e.g. References [15, 18, 32, 33] or Reference [41] for incompatible contact interfaces).

Accepted Manuscript

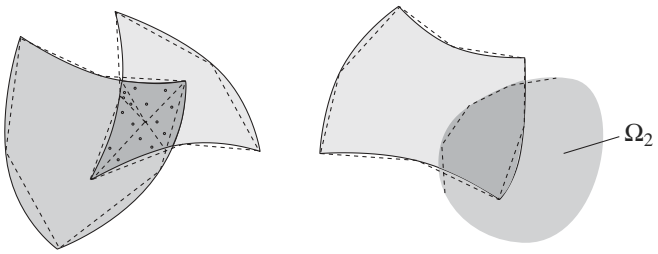

Figure 4. Approximate computation of intersections.

3.3. Integration issue

The adopted solution consists in elaborating more suitable integration rules for each element of the triangulations. Hierarchical procedures can be used. In References [31, 42], we test one such procedure. Despite its simplicity and effectiveness, the associated algorithm seems to be CPU and memory consuming, when 3-D elements are concerned or when the geometrical characteristics of the superimposed triangulations are quite dissimilar. The numerical integration strategies developed by Stouboulis *et al.* [43, 44] could be as well updated to our problem though to our knowledge, the 3-D version of the so-called fast remeshing quadrature algorithm is not available.

We here test an alternative procedure based on the computation of geometric intersections of finite elements. The approach actually consists in partitioning the integration domain into sub-elements where the integrands of (22)–(24) are regular. In this way, (22)–(23) generically read

$$\int_{\Omega_1} \alpha_1 f \, \mathrm{d}\Omega = \sum_{K_1 \in \mathscr{T}_{h_1}} \left(\int_{K_1 \setminus \Omega_2} f \, \mathrm{d}\Omega + \alpha_1^0 \int_{K_1 \cap \Omega_2} f \, \mathrm{d}\Omega \right) \tag{25}$$

and the coupling matrices (24) read

$$\int_{S_g} f \, \mathrm{d}\Omega = \sum_{K_g \in \mathscr{T}_{h_g}} \sum_{K_1 \in \mathscr{T}_{h_1}} \int_{K_g \cap K_1} f \, \mathrm{d}\Omega = \sum_{K_g \in \mathscr{T}_{h_g}} \sum_{K_2 \in \mathscr{T}_{h_2}} \int_{K_g \cap K_2} f \, \mathrm{d}\Omega \tag{26}$$

The above elementary integrals are reduced to classical ones, when in (25), K_1 is located on one side of $\partial\Omega_2$ or in (26), $K_g \subset K_1$ for instance. A large number of computations can hence be saved through the identification of such configurations by elementary geometrical tests (see Reference [42], for details).

For the remaining cases, intersections of element supports are computed. This task is achieved by sampling and triangulating the boundary of the elements and the domains (see Figure 4). The ensuing polyhedra intersection problems are then treated through classical algorithms developed by the computational geometry community (see e.g. References [45, 46]).

Remark 5

When both polyhedra share perfectly coincident parts of faces, the related intersection problem requires quite sofisticated procedures. In that cases, the intersection may indeed be reduced to single points, segments or polygonal surfaces. Since the consideration of such zero measured

Accepted Manuscript

manifolds is irrevelant for our applications, we slightly move each boundary sampling point in a random direction so as to only treat pairs of polyhedra in general position.

3.4. Coupling matrices

We now successively consider the case of (26) then (25). First, to elaborate quadrature rules for the evaluation of coupling matrices terms, the intersection polyhedra are tetrahedralized. This *a priori* intricate geometry problem is solved by assuming that these polyhedra are star shaped around their gravity centres (which can be located through the Green's formula). The tetrahedralization is then built through connecting these centres to each vertices of the polyhedron (see Figure 5 on the left). Note that since usual finite elements are almost convex, this assumption was always verified in our applications.

To further detail the computations, we consider $(K_g,\ K_1) \in \mathscr{T}_{h_g} \times \mathscr{T}_{h_1}$ such that the associated intersection polyhedron be non-zero measured, $(\boldsymbol{\varphi}_g^i,\ \boldsymbol{\varphi}_1^j)$ two finite element basis functions of $\mathbf{W}_{h_g} \times \mathbf{W}_{h_1}$ which supports, respectively, enclose K_g and K_1, and we let $\mathscr{T}_{K_g \cap K_1}$ denote the tetrahedralization of $K_g \cap K_1$. That way, the evaluation of (24) using (26) is generically carried out in the following way:

$$\int_{K_g \cap K_1} \boldsymbol{\varphi}_g^i . \boldsymbol{\varphi}_1^j \, \mathrm{d}\Omega \simeq \sum_{K \in \mathscr{T}_{K_g \cap K_1}} J_{\boldsymbol{\Phi}_K} \sum_{\hat{\mathbf{g}}} \rho_{\hat{\mathbf{g}}} \, (\hat{\boldsymbol{\varphi}}^I \circ \boldsymbol{\Phi}_{K_g}^{-1} \circ \boldsymbol{\Phi}_K)(\hat{\mathbf{g}}) \, . \, (\hat{\boldsymbol{\varphi}}^J \circ \boldsymbol{\Phi}_{K_1}^{-1} \circ \boldsymbol{\Phi}_K)(\hat{\mathbf{g}}) \tag{27}$$

where $\boldsymbol{\Phi}_K$, $J_{\boldsymbol{\Phi}_K}$, $\hat{\boldsymbol{\varphi}}^I$ and $\hat{\boldsymbol{\varphi}}^J$ stand for the mapping between K and the related reference element, its jacobian and the shape functions associated to $\boldsymbol{\varphi}_g^i$ and $\boldsymbol{\varphi}_1^j$, respectively. In addition, $\rho_{\hat{\mathbf{g}}}$ and $\hat{\mathbf{g}}$ denote the weights and points of the appropriate Hammer's integration rule.

To choose these rules when models with different interpolations are superimposed, we follow classical results (e.g. Reference [39]) and assume that the geometric distortion of the elements is weak. That way, the mappings $\boldsymbol{\Phi}_{K_g}$, $\boldsymbol{\Phi}_{K_1}$, $\boldsymbol{\Phi}_{K_2}$ are almost affine, so that the integrands of (24) are close to polynomials for which we can compute degrees and that we can automatically associate to proper quadrature schemes (e.g. Reference [47]).

3.5. Weighting strategy

While this tetrahedralization strategy is appropriate to the evaluation of the coupling matrices, it may not be to compute the weighted virtual works. Indeed, this approach increases the number of integration points, which may lead to prohibitive costs when non-linear or history dependent material are used, and may be tricky with under-integrated elements such as those used for incompressible media or for thin structures. Therefore, we choose to approximate the effect of the weighting functions by their mean value on each finite element. This reads

$$\int_{\Omega_1} \alpha_1 \boldsymbol{\sigma}(\boldsymbol{\varphi}_1^j) : \boldsymbol{\varepsilon}(\boldsymbol{\varphi}_1^k) \, \mathrm{d}\Omega \simeq \sum_{K_1 \in \mathscr{T}_{h_1}} \left(1 - \alpha_2^0 \, \frac{|K_1 \cap \Omega_2|}{|K_1|} \right) \int_{K_1} \boldsymbol{\sigma}(\boldsymbol{\varphi}_1^j) : \boldsymbol{\varepsilon}(\boldsymbol{\varphi}_1^k) \, \mathrm{d}\Omega \tag{28}$$

In this equation, the volume ratio is evaluated by triangulating the boundaries of both K_1 and the polyhedron associated to the intersection of K_1 with Ω_2, and by applying the classical Green's formula. The relevance of this approximation is illustrated by our numerical examples, for which we do not notice any numerical pathology such as spurious stress oscillation around the gluing zone.

Accepted Manuscript

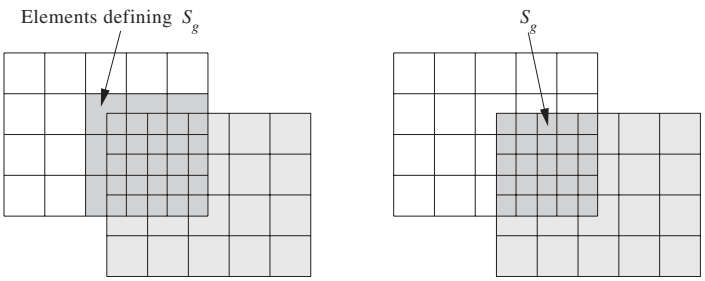

Figure 5. Operational definition of $\mathscr{T}_{h_g}$ and S_g.

3.6. Triangulation of the gluing zone

Up to now, we considered an independent mesh to describe S_g. For our applications, we use a more convenient and theoretically founded choice for which we do not need to explicitly triangulate the gluing zone.

It consists in considering (see Figure 5) a subset of $\mathscr{T}_{h_1}$ (or $\mathscr{T}_{h_2}$) which elements may not be totally included in the overlap, and in describing the gluing zone by the intersection of this subset with Ω_2 (or Ω_1).

No additional developments are then needed, since using (26) in the following way, only the intersections of the elements of $\mathscr{T}_{h_1}$ with Ω_2 are considered for the evaluation of (24):

$$\int_{S_g} f \, \mathrm{d}\Omega = \sum_{K_g \in \mathscr{T}_{h_g} (\subset \mathscr{T}_{h_1})} \sum_{K_2 \in \mathscr{T}_{h_2}} \int_{K_g \cap K_2} f \, \mathrm{d}\Omega \tag{29}$$

However, since $(\mathscr{T}_{h_g})$ is used to discretize the multiplier space, only the elements of $(\mathscr{T}_{h_g})$ which have a *significant* intersection with Ω_2 are considered so as to ensure the stability of the numerical approximation of linear system (21). Finally, note that the choice of the triangulation, $\mathscr{T}_{h_1}$ or $\mathscr{T}_{h_2}$, to define $\mathscr{T}_{h_g}$ affects the solution fields $\mathbf{u}_{h_1}$ and $\mathbf{u}_{h_2}$. This influence is exemplified by a 1-D numerical result in the following section.

4. NUMERICAL EXAMPLES

4.1. Clamped vertical bar loaded by its own weight

We first consider a one-dimensional mechanical problem to compare the stability of the mixed Arlequin formulation when the gluing operator is based on either discretized L^2 or H^1 inner products (see Section 2, Remark 2). Recall that the discrete L^2 inner product approximates the continuous duality bracket between the space of fields of finite energy in the gluing zone and its dual space. The mechanical problem consists in evaluating the vertical displacement field, u, in an upright bar of constant section, clamped at both ends and loaded by its own weight (see Figure 6 on the left).

Its section Σ, its Young's modulus E, its density ρ and the gravity factor g are chosen so that $\rho g = E\Sigma$. In addition, the Arlequin model for this problem consists in the superposition of two equally fine meshes set in $]0, 2[$ and $]1, 3[$ which step is denoted by h. Since the

Accepted Manuscript

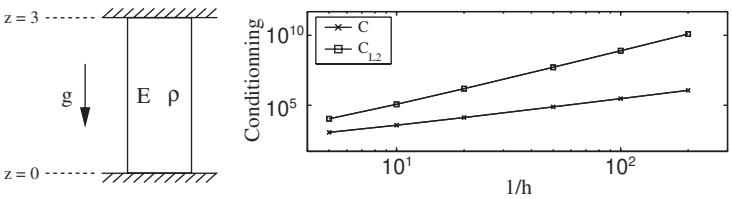

Figure 6. Clamped vertical bar and comparison of the conditioning of (21).

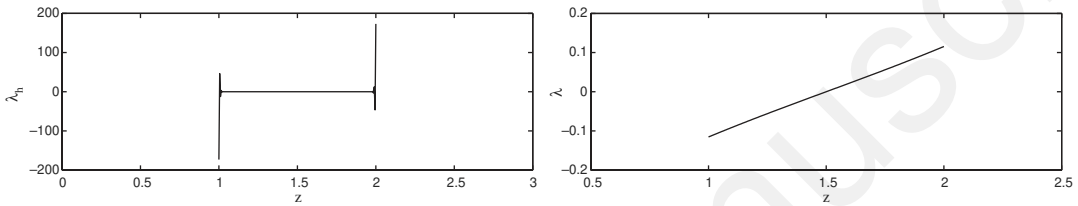

Figure 7. Comparison of solution multiplier fields for $h = 0.05$.

superimposed models are of same refinement, the weight functions α_i and β_i are taken equal to $\frac{1}{2}$ in the gluing zone, coinciding here with the overlap. Continuous 1-D linear elements are used to approximate the displacement and Lagrange multiplier fields.

In Figure 6 on the right, we first compare the influence of the mesh size h on the conditioning of the related linear systems (21). Note that the C coupling operator leads to conditioning numbers varying as $1/h^2$ (which is usual for finite element matrices), whereas the C_{L^2} operator leads to worse conditioning numbers, varying as $1/h^4$.

This deterioration can be related to the very different behaviours of the gluing multiplier field λ_h in both cases. Contrary to C (see Figure 7 on the right), C_{L^2} leads to non-smooth multiplier fields (see Figure 7 on the left). In this case, we indeed observe that with respect to h the gluing forces density tends to be equal to zero almost everywhere in the gluing zone, becoming more and more oscillating in the neighbourhood of the boundary of this gluing zone, with a numerical value on the two points of the boundary varying as $1/h$. Actually it seems to converge toward a distribution (viz. an element of the dual of the kinematical admissible fields space).

The same numerical example is now used to illustrate the influence of the triangulation used to descritize the Lagrange multiplier field on the solution mechanical states. This time, different refinements of the superimposed models are considered. In Figure 8, the resulting discrete displacement fields obtained for $\alpha_2 = 99\%$ (i.e. the α function associated to the finest model) are plotted in the overlap. In addition, the analytical solution displacement field denoted u_{ref} is also represented.

Notice that, depending on whether the gluing forces space is chosen to be equal to the restriction to the glue zone of the finest or the coarsest finite element space, the finest mechanical state is either locked to the coarsest one (left part of Figure 8), or linked to it in an average sense (right part of Figure 8). Both choices may have practical interests.

Author Manuscript

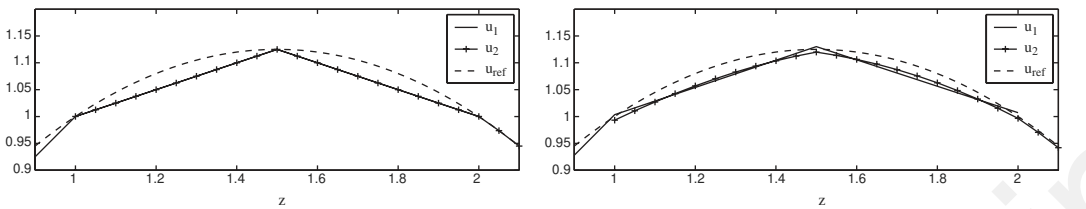

Figure 8. Influence of the triangulation $\mathcal{T}_{h_g}$.

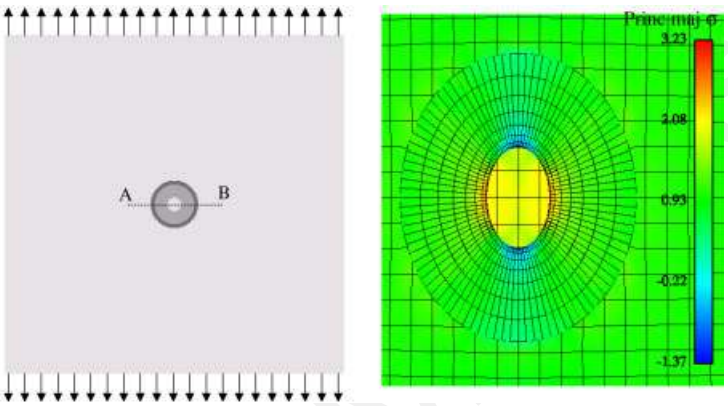

Figure 9. Drilled plate under tension.

4.2. Drilled plate

The next example aims at testing the soundness of the numerical approximations developed in Section 3. We consider the classical linear elasticity problem of a circular hole in an infinite 2-D plate. The infinite plate is approximated by a 20-by-20 square for a $R_0 = 0.4$ radius hole. Planed stress isotropic homogeneous linearized elasticity is assumed.

The test consists in considering independent finite element models for a global plate with no hole and a local one with a hole, and in superimposing them through the Arlequin framework. The global square plate model is submitted to uniform traction loads (denoted σ_∞ and taken here equal to 1) along its upper and lower edges. The local model for the hole consists in a 2.8 diameter circular ring and the gluing zone is defined as the annulus located between radius 1.3 and 1.4 (see Figure 9 on the left).

Here, completely different mechanical models concurrently exist in the superposition zone. In order to obtain the solution of a plate with a hole, the weight is put on the local *drilled* model. Namely the related weight function parameter α^0 is set to 99.9%.

The meshes of the superimposed models are independent so as to treat non-trivial geometrical configurations. The global one is regular and its step is denoted by h. In the sequel, several refinement levels are considered for both models, and parameter h is used to quantify these levels.

The right part of Figure 9 shows a zoom around the hole depicting the deformed meshes and the related iso-major principal stress field obtained for $h = \frac{1}{4}$. For the superimposed meshes

Accepted Manuscript

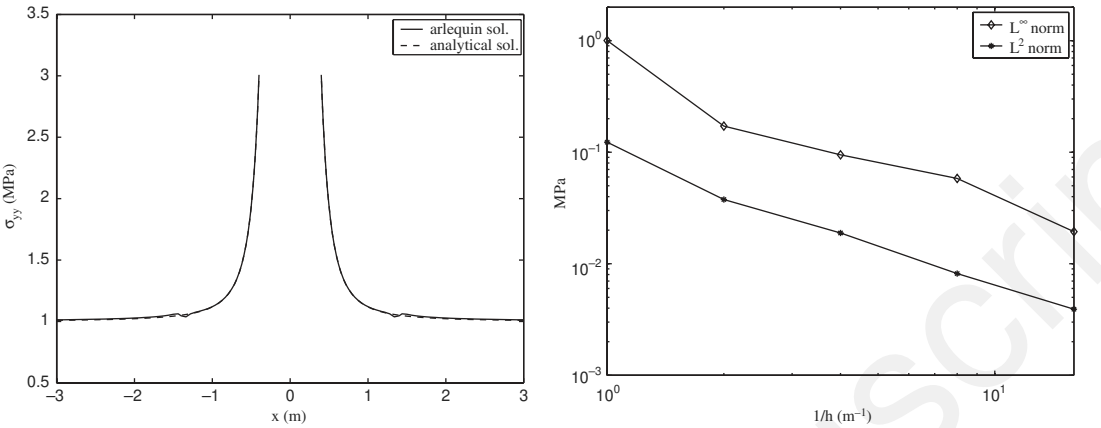

Figure 10. Comparison between the Arlequin solution and the analytical one for an infinite plate.

are quite incompatible, note that no significant spurious stresses oscillations can be observed around the gluing zone.

This remark can be also supported through comparing the smoothed *Arlequin* stress tensor component σ_{yy}^{arl} (see Remark 1) along segment AB (see Figure 9 on the left) to the analytically known solution related to the infinite plate. Letting r denote the distance from the hole centre, this solution reads:

$$\sigma_{yy}^{\text{ana}} = \sigma_\infty \left(1 + \frac{1}{2}\left(\frac{R_0}{r}\right)^2 + \frac{3}{2}\left(\frac{R_0}{r}\right)^4\right) \tag{30}$$

Both curves are plotted in Figure 10 on the left for $h = \frac{1}{16}$.

First note the well known stress concentration factor 3 found on the boundary of the hole. Secondly remark the small numerical oscillation of the stress field in the gluing zone. As a matter of fact, this oscillation is related to the geometrical incompatibility of the meshes, to their different finenesses and to the size of the superposition zone.

In order to consider the influence of the mesh size parameter h, a logarithmic error analysis is plotted in Figure 10 on the right, where the considered error measures are defined as follows:

$$L^\infty\text{error} = \max_{AB} |\sigma_{yy}^{\text{arl}} - \sigma_{yy}^{\text{ana}}| \tag{31}$$

$$L^2\text{error} = \left(\frac{1}{|AB|}\int_{AB} (\sigma_{yy}^{\text{arl}} - \sigma_{yy}^{\text{ana}})^2 \, \mathrm{d}s\right)^{1/2} \tag{32}$$

These results show in particular the relevance of the numerical approximations and integration strategies developed in Section 3 for the operational implementation.

Accepted Manuscript

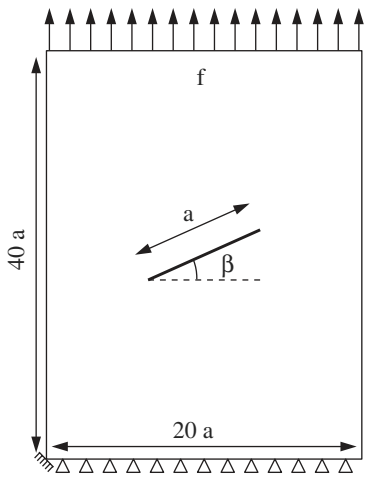

Figure 11. Slant cracked plate under tension.

4.3. Slant cracked plate under tension

The second 2-D test aims at illustrating both the accuracy and the effectiveness of the Arlequin approach to locally change a global model. The mechanical test consists in a plate with a crack with length a and inclined with angle β, submitted to a uniform traction density of loads $f = 100$ MPa and assumed to be in plane stress. This test is depicted in Figure 11. In this benchmark, engineering quantities of interest are also analytically known when the plate is infinite. Namely, the expressions of the energy release rate G and the first and second intensity factors K_{I} and K_{II} are, respectively, given by (33)–(35).

$$G = \frac{f^2}{E} \pi a \cos^2 \beta \tag{33}$$

$$K_{\mathrm{I}} = f\sqrt{\pi a} \cos^2 \beta \tag{34}$$

$$K_{\mathrm{II}} = f\sqrt{\pi a} \sin \beta \cos \beta \tag{35}$$

This case is treated through the Arlequin framework by superimposing a very local cracked model to the global plate one. The used meshes for the global model and the local cracked one are depicted in Figure 12 where the tinted area stands for the chosen gluing zone. Moreover we have taken $a = 1$ mm and $\beta = 37°$, with a Young's modulus and a Poisson ratio equal to 200 GPa and 0.3, respectively.

The resulting deformed numerical Arlequin model in local zones of interest, and the major principal stresses field, obtained for $\alpha^0_{\mathrm{crack}} = 99.99\%$, are given in Figure 13. Notice that $\alpha^0_{\mathrm{crack}}$ here refers to the weight function parameter associated to the local cracked model. The one associated to the global model is denoted by $\alpha^0_{\mathrm{plate}}$. Recall that by definition $\alpha^0_{\mathrm{crack}} + \alpha^0_{\mathrm{plate}} = 1$.

The values of energy release rates and stress intensity factors obtained with higher and higher weight on the cracked model are compared to the analytical values holding for an infinite plate

Accepted manuscript

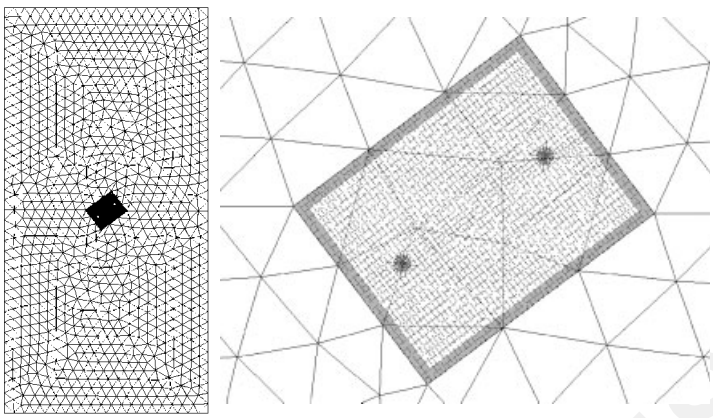

Figure 12. Meshes of the global and the local cracked plates.

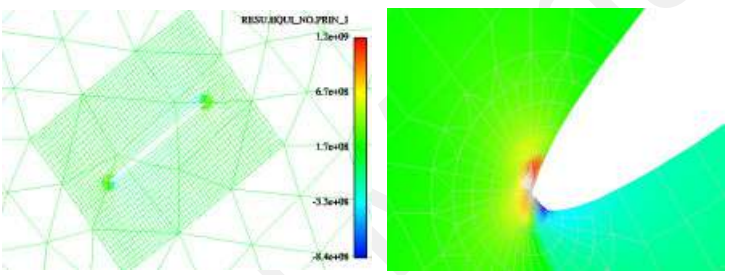

Figure 13. Deformed meshes and major principal stress field.

and to the values obtained by a similarly refined classical finite element (mono)model (see Figures 14 and 15). For the particular numerical test considered here, it is even possible to take $\alpha^0_{\text{plate}} = 0$. The related values of the same mechanical quantities are also given in Figures 14 and 15 and labelled *limit Arlequin solution*.

Note that although only locally refined, the numerical results obtained by the Arlequin approach (when the weight is significantly put on the local refined model) are as accurate as the ones obtained by a similarly (but globally) refined classical finite element (mono)model.

4.4. Bending of a pipe elbow

The Arlequin framework is used in the following examples to couple a local 3-D model to a shell one. The 3D-Shell discrete partition is derived from the continuous Arlequin problem (5) in a rather straightforward way. Basically one has to approximate one of the two models (say model 2, the one defined in Ω_2) by a shell model. The obtained (still) continuous problem can be discretized by means of solid finite elements used to approximate model 1 and of appropriate shell finite elements for model 2. The gluing zone is described by a volume in which the displacement shell fields are unambiguiously defined so as to be glued to the 3D displacement fields. In addition, the space of gluing forces is taken as the restriction to the

Accepted manuscript

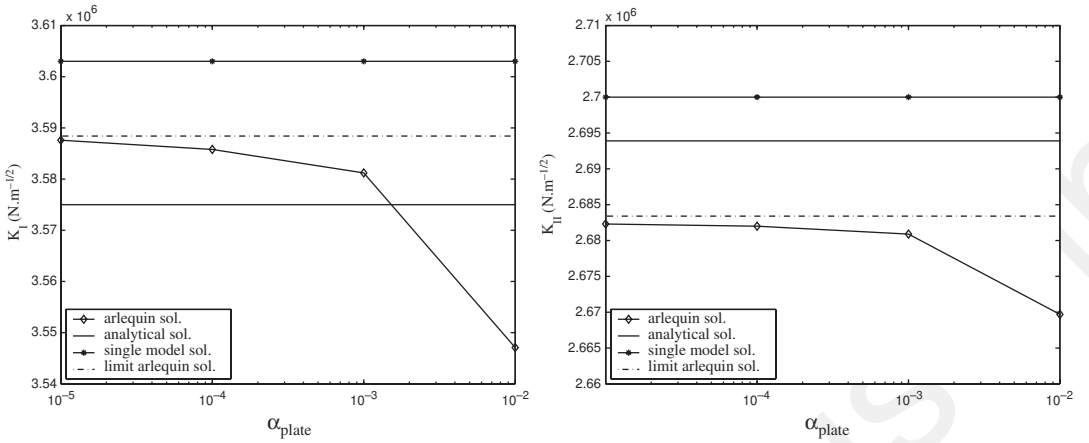

Figure 14. Stress intensity factors K_{I} and K_{II}.

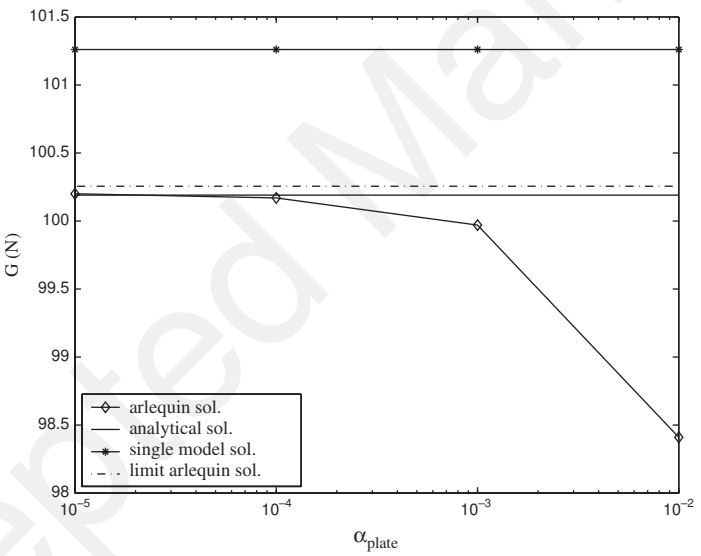

Figure 15. Energy release rate.

gluing zone of the space of kinematical shell fields. The reader is referred to References [48, 42, 49] for more details related to this important type of coupling in the computational mechanics field.

The mechanical problem illustrating here this aspect consists in the bending of a right-angle pipe elbow. In the Arlequin framework, a 3-D local model is used to discretize the mechanical states in the bend, while shell global ones are used for the right parts of the pipe. This geometry is depicted in Figure 16. Linearized elasticity is assumed. The Young's modulus and

Accepted Manuscript

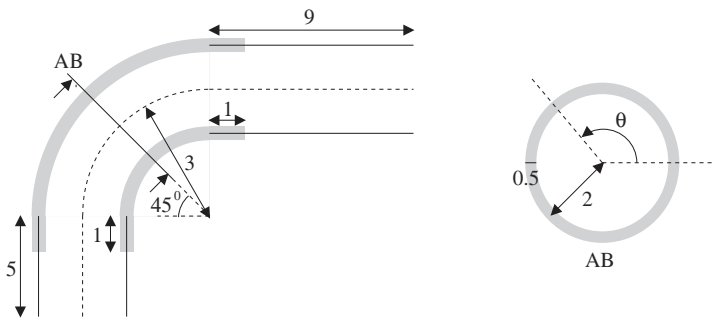

Figure 16. Right-angle pipe elbow geometry.

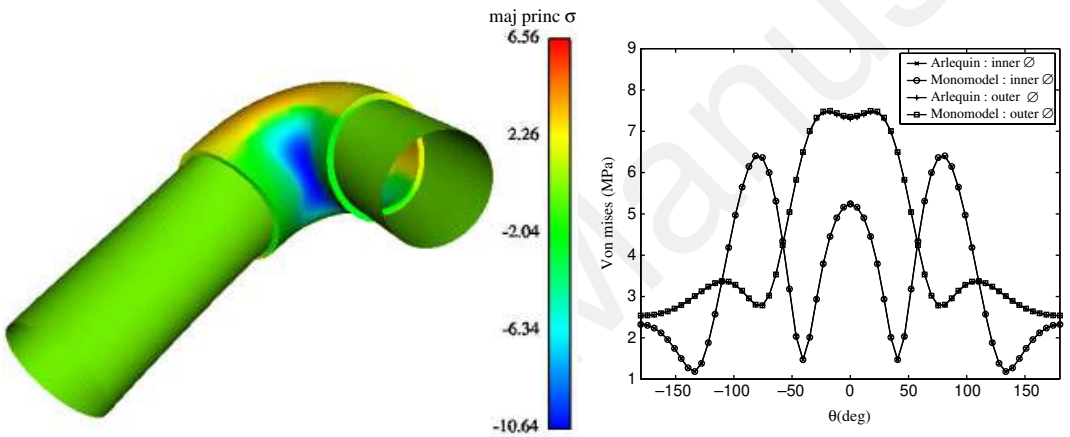

Figure 17. Bending of a right-angle pipe elbow.

the Poisson ratio are, respectively, equal to 300 GPa and 0.3. One end related to the shortest pipe arm is clamped while the other end is submitted to uniform displacement.

In Figure 17 on the left, external iso-major principal stress field is shown on the deformed structure. In order to assess the accuracy of the Arlequin solution, the Von-Mises field along the inner and outer perimeter of section *AB* bisecting the elbow (see Figure 16) is compared to the one obtained by a 3-D monomodel (see Figure 17 on the right). The two solutions merely overlap.

With this test, it is believed that the geometrical tools developed in Section 3 are validated in the 3-D space.

5. CONCLUDING REMARKS

In this paper, we worked out numerical strategies in order to mix very different finite element models by the Arlequin method. The effectiveness of these developments have been illustrated

Accepted manuscript

through 1-, 2- and 3-D mechanical tests. That way, we show high potentialities of this modelling framework in term of flexibility and of practical capabilities to locally integrate small defects and low scale mechanical phenomena in numerical models of engineering structures.

The Arlequin framework has also been used to treat contact problems such as the Boussinesq one for which the stress tensor is locally singular [41]. Other mechanical problems can be addressed in this framework. Two of them are now being in progress, namely impact problems [50] and the important field involving the dynamic coupling of discrete/continuum mechanics (e.g. Reference [51]) for which at least the gluing operator has to be re-analysed.

Some aspects directly or indirectly related to the approach have however to be investigated more deeply. We mention in particular the optimal practical choice of the weighting parameter functions, the definition (through adaptive approaches) of optimal sizes and refinements of the superposition and gluing zones relatively to the size and refinement of the underlying global model and the multiple superposition procedure which is essential for a multiscale analysis.

ACKNOWLEDGEMENTS

The support of Électricité de France is gratefully acknowledged.

REFERENCES

1. Nayroles B, Touzot G, Villon P. Generalizing the finite element method: diffuse approximation and diffuse elements. *Computers and Structures* 1992; **10**(5):307–318.
2. Belytschko T, Lu YY, GU L. Element-free Galerkin methods. *International Journal for Numerical Methods in Engineering* 1994; **37**:229–256.
3. Belytschko T, Organ D, Krongauz Y. A coupled finite element-element-free Galerkin method. *Computational Mechanics* 1995; **17**:186–195.
4. Hughes TJR. Multiscale phenomena: Green's functions, the Dirichlet-to-Neumann formulation, subgrid scale models, bubbles and the origin of stabilized methods. *Computer Methods in Applied Mechanics and Engineering* 1995; **127**:387–401.
5. Hughes TJR, Feijóo GR, Mazzei L, Quincy JB. The variational multiscale method—a paradigm for computational mechanics. *Computer Methods in Applied Mechanics and Engineering* 1998; **138**:3–24.
6. Zohdi TI, Oden JT, Rodi GJ. Hierarchical modelling of heterogeneous bodies. *Computer Methods in Applied Mechanics and Engineering* 1996; **138**:273–298.
7. Oden JT, Zohdi TI. Analysis and adaptative modelling of highly heterogeneous elastic structures. *Computer Methods in Applied Mechanics and Engineering* 1997; **148**:367–391.
8. Melenk JM, Babuška I. The partition of unity finite element method. Basic theory and applications. *Computer Methods in Applied Mechanics and Engineering* 1996; **139**:289–314.
9. Babuška I, Melenk JM. The partition of unity method. *International Journal for Numerical Methods in Engineering* 1997; **40**:727–758.
10. Babuška I, Strouboulis T, Copps K. The design and analysis of the generalized finite element method. *Computer Methods in Applied Mechanics and Engineering* 2000; **181**:43–69.
11. Belytschko T, Black T. Elastic crack growth in finite-elements with minimal remeshing. *International Journal for Numerical Methods in Engineering* 1999; **745**:601–620.
12. Moës N, Dolbow J, Belytschko T. A finite element method for crack growth without remeshing. *International Journal for Numerical Methods in Engineering* 1999; **746**:131–150.
13. Sukumar N, Moës N, Moran B, Belytschko T. Modeling holes and inclusions by level sets in the extended finite element method. *Computer Methods in Applied Mechanics and Engineering* 2000; **48**:1549–1570.
14. Kim HG. Arbitrary placement of local meshes in global mesh by the interface-element method (IEM). *International Journal for Numerical Methods in Engineering* 2003; **56**:2279–2312.
15. Fish J. The s-version of the finite element method. *Computers and Structures* 1992; **43**:539–547.

Accepted Manuscript

16. Belytschko T, Fish J, Bayliss A. The spectral overlay on finite elements for problems with high gradients. *Computer Methods in Applied Mechanics and Engineering* 1990; **81**:71–89.
17. Fish J, Markolefas S. The s-version of the finite element method for multilayer laminates. *International Journal for Numerical Methods in Engineering* 1992; **33**:1081–1105.
18. Fish J, Markolefas S. Adaptive s-method for linear elastostatics. *Computer Methods in Applied Mechanics and Engineering* 1993; **104**:363–396.
19. Fish J, Aditya N. Adaptive and hierarchical modelling of fatigue crack propagation. *International Journal for Numerical Methods in Engineering* 1993; **36**:2825–2836.
20. Ben Dhia H. Multiscale mechanical problems: the Arlequin method. *Comptes Rendus de l'Académie des Sciences Série IIb* 1998; **326**:899–904.
21. Ben Dhia H. Numerical modelling of multiscale problems: the Arlequin method. *CD Proceedings of ECCM'99*, Munchen, 1999.
22. Raviart PA, Thomas JM. Primal hybrid finite element methods for second order elliptic equations. *Mathematics of Computation* 1977; **31**:391–396.
23. Farhat C, Roux FX. A method of finite element tearing and interconnecting and its parallel solution algorithm. *International Journal for Numerical Methods in Engineering* 1991; **32**:1205–1227.
24. Le Tallec P. Domain decomposition methods in computational mechanics. *Computational Mechanics Advances* 1994; **1**(2):121–220.
25. Steger JL, Benek JA. On the use of composite grid schemes in computational aerodynamics. *Computer Methods in Applied Mechanics and Engineering* 1987; **64**:301–320.
26. Lions JL, Pironneau O. Domain decomposition methods for CAD. *Comptes Rendus de l'Académie des Sciences Série I* 1999; **328**:73–80.
27. Le Dret H. *Problèmes Variationnels dans les Multidomaines. Modélisation des Jonctions et Applications*. Masson: Paris, 1991.
28. Ciarlet PG. *Mathematical Elasticity*: *Theory of Plates*, vol. II. Elsevier: New York, 1997.
29. Abraham FF, Broughton JQ, Benrnstein N, Kaxiras E. Spanning the length scales in dynamic simulation. *Computers in Physics* 1998; **12**:538–546.
30. Ben Dhia H, Rateau G. Mathematical analysis of the mixed Arlequin method. *Comptes Rendus de l'Académie des Sciences Paris Série I* 2001; **332**:649–654.
31. Ben Dhia H, Rateau G. Application of the Arlequin method to some structures with defects. *Revue Européenne des éléments finis* 2002; **11**(2-3-4):291–304.
32. Kazabeau L, Maday Y, Lacour C. Numerical quadratures and mortar methods. *Computational Sciences in the 21st Century*. Wiley: New York, 1997; 534–542.
33. Maday Y, Rapetti F, Wohlmuth BI. Coupling between scalar and vector potential by the mortar element method. *Comptes Rendus de l'Académie des Sciences*, *Paris* 2001; **334**:933–938.
34. Gurtin ME. *An Introduction to Continuum Mechanics*. Academic Press: New York, 1981.
35. Rudin W. *Functional Analysis*. McGraw-Hill: New York, 1973.
36. Bernardi C, Maday Y, Patera A. A new nonconforming approach to domain decomposition: the mortar element method. In *College de France Seminar*, Brezis H, Lions J (eds). Pitman: Boston, MA, 1990.
37. Ben Belgacem F. The mortar finite element method with Lagrange multipliers. *Numerische Mathematik* 1999; **84**:173–197.
38. Cai XC, Dryja M, Sarkis M. Overlapping nonmatching grid mortar element methods for elliptic problems. *SIAM Journal on Numerical Analysis* 1999; **36**:581–606.
39. Ciarlet PG. *The Finite Element Method for Elliptic Problems*. North-Holland: Amsterdam, 1978.
40. Glowinski R, Pan TW, Hesla T, Joseph D, Periaux J. A distributed Lagrange multiplier/fictituous domain method for the simulation of flow around moving rigid bodies: application to particle flow. *Computer Methods in Applied Mechanics and Engineering* 2000; **184**:241–267.
41. Ben Dhia H, Zarroug M. Contact in the Arlequin framework. In *Contact Mechanics*, Martins JAC, Monteiro Marques MDP (eds). Kluwer Academic Publishers: Dordrecht, 2001; 401–410.
42. Rateau G. Méthode Arlequin pour les problèmes mécaniques multi-échelles. Application à des problèmes de Jonction et de fissuration de structures élancées. *Ph.D.*, Ecole Centrale Paris, 2003. http://www.mssmat.ecp.fr/resultat/theses/pdf/these_rateau.pdf
43. Strouboulis T, Copps K, Babuška I. The generalized finite element method: an example of its implementation and illustration of its performances. *International Journal for Numerical Methods in Engineering* 2000; **47**:1401–1417.

Accepted Manuscript

44. Strouboulis T, Copps K, Babuška I. The generalized finite element method. *Computer Methods in Applied Mechanics and Engineering* 2001; **190**:4081–4193.
45. Mehlhorn K, Simon K. Intersecting two polyhedra, one of which is convex. In *Proceedings of Fundamentals of Computation Theory*, vol. 199. Springer: Berlin, 1985; 534–542.
46. O'Rourke J. *Computational Geometry in C*. Cambridge University Press: Cambridge, 1994.
47. Zienkiewicz OC, Taylor RLG. *The Finite Element Method*, vols. 1, 2. McGraw-Hill: New York, 1999, 2001.
48. Ben Dhia H, Durand C, Rateau G. Partition 3D-coque par la méthode Arlequin. *Proceedings of Colloque National en Calcul des Structures 6*, vol. III. 2003; 263–270. http://www.mssmat.ecp.fr/structures/REFERENCE/pdf/rateeau_coque3d.pdf
49. Ben Dhia H, Rateau G. The Arlequin method as a multiscale mechanical tool. *CD Proceedings of WCCMVI*, Beinjing, China, 5–10 September 2004.
50. Ben Dhia H, Zammali C, Lamarche S, Voldoire F. Modèles et schémas mixtes pour le contact en dynamique *Proceedings of Colloque National en Calcul des Structures 6*, vol. I. 2003; 385–392.
51. Xiao SP, Belytschko T. A bridging domain method for coupling continua with molecular dynamics. *Computer Methods in Applied Mechanics and Engineering* 2004; **193**:1645–1669.

Accepted Manuscript